Memoirs of the Faculty of Engineering, Nagoya University
Vol. 35, No. 1 (1983)

FLOW IN AXIALLY ROTATING PIPES

MITSUKIYO MURAKAMI, KOJI KIKUYAMA,
and KENJI NISHIBORI

Department of Mechanical Engineering

(Received May 31, 1983)

Abstract

This paper describes the flow pattern, hydraulic resistance, and stability of flows in axially rotating pipes. Developed and undeveloped flows, respectively, were introduced to smooth pipes rotating about their axes, and changes of flow pattern, hydraulic losses, and turbulent fluctuations due to the rotation were measured across sections at various distances from the pipe entrance. The pipe rotation gives two counter effects on the flow: one is a destabilizing effect due to a large shear caused by the rotating pipe wall and the other is a stabilizing effect due to the centrifugal force of the swirling velocity component. The different effects of the pipe rotation on the flow stability are attributable to the flow condition at the inlet section and also to the boundary layer development. The stability effect can be predicted theoretically by use of a relationship between the mixing length and Richardson number proposed by Bradshaw.

CONTENTS

1. Experiments on the Flow in Fully Developed Region

1. 1. Introduction

When fluid enters a pipe rotating about its axis, tangential forces acting between the rotating pipe wall and the fluid cause the fluid to rotate with the pipe, resulting in a rather different flow pattern from that observed in the stationary pipe. Examples are found in several engineering applications; for example, in the inlet part of fluid machines, heat exchangers, and cooling systems of rotors.

Profiles of flow velocity in a rotating pipe were analyzed by Lavan and his co-workers[1], when a fully developed laminar flow was introduced to an axially rotating pipe. A reverse flow was found in the wall region near the inlet section when the swirl rate, defined by the ratio of the tangential velocity of the rotating pipe to the mean axial flow velocity, was sufficiently large.

By measuring the static pressure difference between two pressure tappings

located upstream and downstream of rotating pipes, White[2], Levy[3], and Щукин[4] studied pressure losses in rotating pipes. The magnitude of the loss varies considerably with the swirl rate. As the rotating speed is increased, the loss is increased if the approaching flow is laminar, but is decreased if the approaching flow is turbulent.

By employing a flow visualization technique, Cannon and Kays[5] found that there were two regions in the rotating sections when the swirl rate was sufficiently high — one was a rotating region near the pipe wall, and the other a nonrotating one enclosed in it. It was also found that in the rotating layer the turbulence was suppressed and the burst of turbulence on the boundary of the two regions was diminished with increase of swirl rate.

For turbulent flows in a rotating pipe, Борисенко, et al.[6] measured turbulence intensities by use of hot wire probes and showed that they were suppressed by rotation and that the suppression extended to the central portion of section as the flow proceeded downstream.

Pedley[7] theoretically analyzed the stability of laminar flow in a long pipe and found it unstable at a constant axial flow Reynolds number of 82.9. By using a visualization technique and a hot thermister anemometer, Nagib and his coworkers[8] also confirmed that when a solid body rotation was superposed on an axial velocity profile having a characteristic of a saturated laminar flow, the rotation destabilized the flow. The transition Reynolds number decreased continuously as the swirl rate of the flow increased to $N=4$, and when the swirl rate exceeded this value, the ideal, solid body rotation profile could not be observed.

Apparently rotation has two counter effects on the flow, stabilizing or destabilizing according to the flow conditions in the rotationg pipe. This chapter is concerned with determination of the governing parameters, the vector velocity fields, and loss coefficients, details of which have been reported in a thesis[9]. Turbulent flow developed fully in a stationary pipe was introduced to rotating straight pipes, and velocity and pressure distributions were measured. Hydraulic losses due to the pipe rotation were found to be closely related to the flow patterns in the rotating pipes.

1. 2. Equipment and Method of Experiment

A schematic outline of the experimental equipment is shown in Fig. 1. 1. Water delivered from the overflow tank was rectified by a honeycomb and led successively to the upstream stationary pipe, rotating pipe, and downstream stationary pipe. The rate of flow was measured by an orifice, as shown. The length of the upstream stationary pipe was $60d$ or more, in order to obtain a fully developed velocity distribution at the rotating pipe entrance, and the length of the downstream stationary pipe was $200d$. Six different rotating pipe lengths were used, namely $30d$, $50d$, $70d$, $120d$, $140d$, and $160d$. The pipes used were drawn brass tubes having a hydraulically smooth surface.

To obtain the overall pressure loss across a rotating pipe, the upstream tapping was placed $10d$ upstream from the rotating section. The downstream tapping was situated $120d$ downstream from it (a pipe length necessary for velocity profile recovery was found experimentally to be about $120d$).

The rotating pipe was separated in two parts by a narrow stationary ring of 5 mm length, as shown in the inset of Fig. 1. 1. The ends of the rotating parts

were supported by ball bearings, and to prevent vibrations due to the rotation the pipe was supported by a series of bearings located at intervals of $20d$ or $30d$. A cylindrical three-hole pitot tube of 2 mm diameter was inserted in the rotating pipe through small holes drilled on the stationary ring, and traversed along the diametral direction to obtain vector profiles across the section.

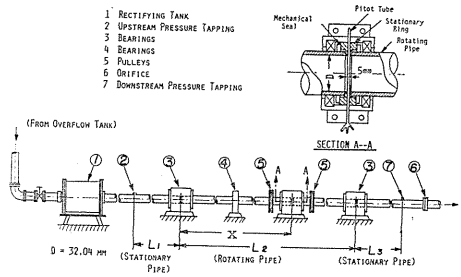

Fig. 1. 1 Schematic outline of experimental equipement.

The moving pipes on both sides of the stationary ring were driven at the same speed by a variable speed motor through belts and pulley systems. Mechanical seals were used for the junctions between the pipes and the ring to prevent any leakage. The experimental range of the axial flow Reynolds number was $10^4 \leqq R_e \leqq 2.0\times10^5$, and the rotational Reynolds number was $0 \leqq R_{ew} \leqq 6.5\times10^4$.

1. 3. Equations to Predict Experimental Results

The overall hydraulic head loss between two pressure tappings, ② and ⑦ as shown in Fig. 1. 1, was measured at various speeds of rotation and flow rate, and is expressed as

$$H=H_1+H_3+H_2=\lambda\frac{L_1+L_3}{d}\cdot\frac{U_m^2}{2g}+\xi\frac{L_2}{d}\cdot\frac{U_m^2}{2g} \tag{1.1}$$

Thus, the coefficient of hydraulic loss of a rotating pipe, ξ, is given by

$$\xi=\left[H-\lambda\frac{(L_1+L_3)}{d}\cdot\frac{U_m^2}{2g}\right]\Big/\left(\frac{L_2}{d}\frac{U_m^2}{2g}\right) \tag{1.2}$$

The hydraulic gradient along the rotating and stationary pipes is schematically shown by a solid line in Fig. 1. 2. It is seen that the first term in the right-hand side of Eq. (1. 1) expresses the hydraulic loss in the stationary pipes upstream and downstream of the rotating pipe, (H_1+H_3), when the swirling flow component is absent. The second term sums the loss in the rotating pipe itself (H_r) and additional loss (H_a) due to the swirling flow components in the downstream stationary pipe.

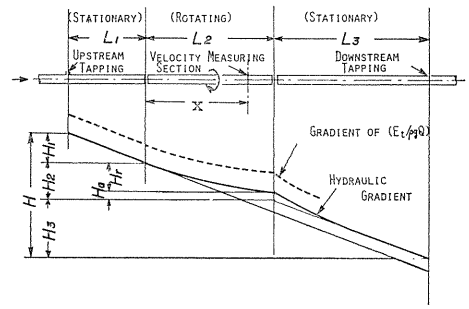

Fig. 1. 2 Change of head along the pipe axis.

If the fluid is considered to be incompressible, and the kinetic energy of eddies is neglected, the sum of the useful mechanical energy of the fluid can be defined by

$$E_t=E_k+E_p \tag{1.3}$$

where E_k and E_p denote fluxes of the kinetic and pressure energies of fluid

$$E_k=\int_0^a 2\pi\rho rU[(U^2+V^2+W^2)/2]dr \tag{1.4}$$

$$E_p=\int_0^a 2\pi Ur(P-P_0)dr \tag{1.5}$$

in which P_0 and P denote the static pressure at the inlet section of the rotating pipe and at any point within a downstream section, respectively.

A balance of the surface stresses and momentum fluxes for a control volume of radius r and length dx as shown in Fig. 1. 3 gives

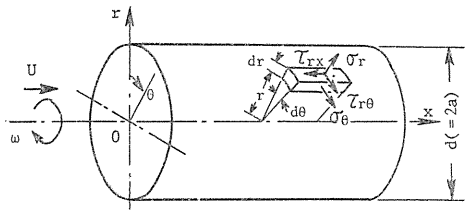

Fig. 1. 3 Cylindrical coordinate system

$$\frac{\tau_{r\theta}}{\rho U_m^2/2}=2\frac{W}{U_m}\cdot\frac{V}{U_m}+\frac{2}{(r/a)^2}\int_0^{r/a}\left(\frac{r}{a}\right)^2\frac{\partial}{\partial(x/a)}\left[\frac{V}{U_m}\cdot\frac{U}{U_m}\right]d\left(\frac{r}{a}\right) \tag{1.6}$$

$$\frac{\tau_{rx}}{\rho U_m^2/2}=2\frac{W}{U_m}\cdot\frac{U}{U_m}+\frac{2}{r/a}\int_0^{r/a}\frac{r}{a}\frac{\partial}{\partial(x/a)}\left[\left(\frac{U}{U_m}\right)^2+\frac{P}{\rho U_m^2}\right]d\left(\frac{r}{a}\right) \tag{1.7}$$

where it is assumed that the flow is taken to be steady, incompressible and axi-symmetric, and also that $\sigma_x\fallingdotseq -P$ and $|\tau_{r\theta}|\ll\rho VU$. The last assumption will be justified from the fact that, in a rotating pipe, the turbulence will be suppressed much by the rotation as is mentioned already and its contribution to the shearing streses can be considered much less than those in a stationary pipe. Since W and U reduce to zero on the pipe wall, the values of $\tau_{r\theta}$ and τ_{rx} on the wall are given by

$$\frac{(\tau_{r\theta})_0}{\rho U_m^2}=2\int_0^1\left(\frac{r}{a}\right)^2\frac{\partial}{\partial(x/a)}\left[\frac{V}{U_m}\frac{U}{U_m}\right]d\left(\frac{r}{a}\right) \tag{1.8}$$

$$\frac{(\tau_{rx})_0}{\rho U_m^2}=2\int_0^1\left(\frac{r}{a}\right)\frac{\partial}{\partial(x/a)}\left[\left(\frac{U}{U_m}\right)^2+\frac{P}{\rho U_m^2}\right]d\left(\frac{r}{a}\right) \tag{1.9}$$

The rate of pipe rotation is defined by the ratio of the circumferential velocity of the pipe to the mean flow velocity as

$$N=V_0/U_m=R_{ew}/R_e \tag{1.10}$$

From Eqs. (1.8) and (1.10), $(\tau_{r\theta})_0/(\rho U_m^2/2)$ can be expressed by

$$\frac{(\tau_{r\theta})_0}{\rho U_m^2/2}=2N\int_0^1\left(\frac{r}{a}\right)^2\frac{\partial}{\partial(x/a)}\left[\frac{V}{V_0}\cdot\frac{U}{U_m}\right]d\left(\frac{r}{a}\right) \tag{1.11}$$

The static pressure at any point, P, can be calculated approximately by the following equation which neglects the radial mean velocity and turbulent fluctuations

$$P=P_w-\rho\int_a^r (V^2/r)dr \tag{1.12}$$

1. 4. Results of Experiments and Discussion

1. 4. 1. Loss Coefficient in Rotating Pipes.

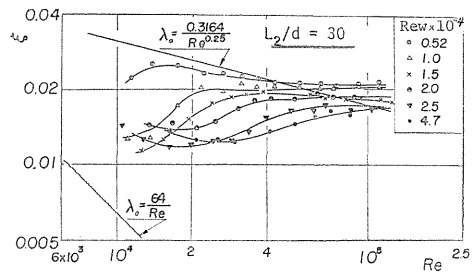

(a) $L_2/d=30$

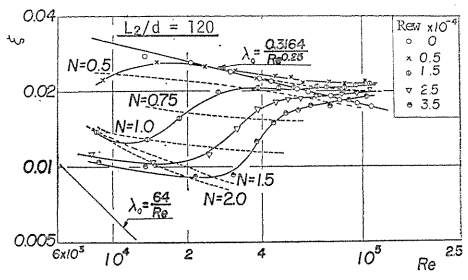

(b) $L_2/d=70$

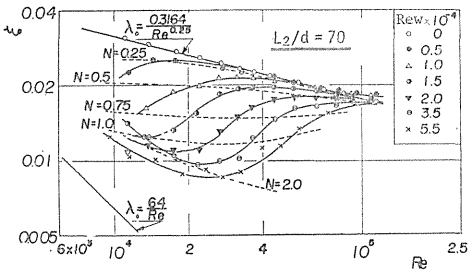

(c) $L_2/d=120$

Fig. 1. 4 Loss coefficients in rotating pipe.

Data for the coefficient of hydraulic loss, ξ, for various lengths of rotating ducts are shown in Figs. 1. 4 (a), (b), and (c). The Reynolds number was always larger than 10^4, so the flow is turbulent when the pipes are held stationary. Therefore, for $N=0$, the curves of ξ will coincide with those for a smooth stationary pipe, λ_0, approximated by the Blasius equation, $\lambda_0=0.3164\ R_e^{-0.25}$. When rotation begins, it is seen that ξ deviates gradually from λ_0, decreasing with increase of rotational speed, R_{ew}, if $R_e<4\times10^4$. This results from suppression of turbulent motion by the swirling flow component. For short rotating tubes, such as $L_2/d=30$, the reduction is less than that for $L_2/d=70$ and above, and the rate of reduction is not consistent with the increase of rotational Reynolds number when $R_e<3\times10^4$.

When R_e is reduced, the value of ξ also decreases continuously to a minimum, and then increases again. To the left of the minimum points, the curves of ξ tend to be parallel asymptotically to the laminar line, $\lambda_0=64/R_e$; turbulence in the flow will be largely suppressed so that viscous effects become dominant. If the rotational Reynolds number, R_{ew}, kept constant and the flow Reynolds number, R_e, is

increased, the values of ξ increase continuously, ultimately exceeding the turbulent friction coefficient of a stationary pipe. The loss caused by the rotating pipe is considered to be composed of the loss experienced in the rotating pipe and an additional loss due to the swirling flow component in the downstream stationary pipe, as shown in Fig. 1. 2. The pipe rotation has an opposite influence on these component losses: the loss within the rotating pipe is decreased but the loss in the stationary pipe downstream of the rotating section is increased. For small rotation rates, the decrease is less than the increase, and ξ becomes larger than λ_0.

When the rotation rate, N, is increased from a small value, the curves of constant N lie at first nearly parallel to the turbulent λ_0 line, then deviate gradually from it and tend to be horizontal. But for $N>1.0$, the curves tend to be parallel to the laminar λ_0 line.

Values of ξ relative to λ_0 are shown against the rotation rate, N, in Figs. 1. 5 (a) and (b). For $N<0.35$, though ξ/λ_0 is slightly larger than 1.0, the effects of

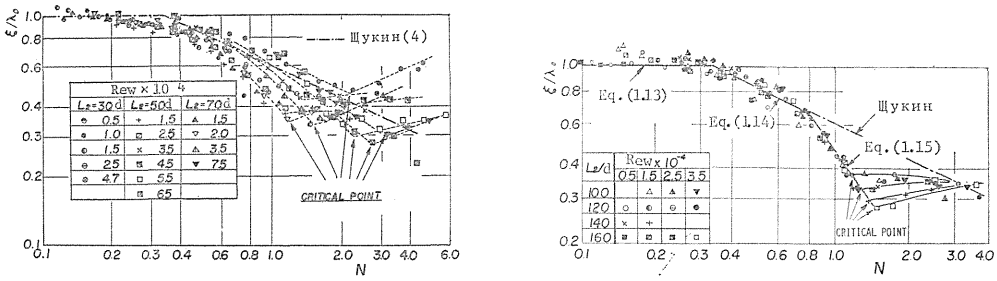

(a) L_2/d=30, 50, and 70 (b) L_2/d=100, 120, 140, and 160

Fig. 1. 5 Relation between ξ/λ_0 and N.

pipe rotation on ξ/λ_0 are negligible. ξ/λ_0 decreases with increase of N and reaches to a minimum value which depends on L_2/d. Scattering of the experimental points increases as the rotating length, L_2, decreases, as is seen in Fig. 1. 5 (a), but this scattering becomes less and ξ/λ_0 becomes almost independent of the pipe length when L_2/d exceeds 100 (Fig. 1. 5 (b)). The relationships between ξ/λ_0 and N, for $L_2/d \geqq 100$, may be approximated by the following equations:

$$\text{for} \quad N<0.35, \quad \xi/\lambda_0=1.0 \tag{1.13}$$

$$\text{for} \quad 0.35 \leqq N \leqq 0.8, \quad \xi/\lambda_0=0.579N^{-0.52} \tag{1.14}$$

$$\text{for} \quad 0.8<N<1.2, \quad \xi/\lambda_0=0.47N^{-1.42} \tag{1.15}$$

In Figs. 1. 5 (a) and (b) the results obtained by Щукин[4] by using the experimental data of White (L_2/d=232) and Levy (L_2/d=24) are also shown by a chain line, which exhibits nearly an upper limit of the present results.

With high speed rotation, $N>1.2$, turbulence in the wall region of the rotating pipe will be largely suppressed, and ξ/λ_0 stops decreasing for larger values of N. Values of the critical flow Reynolds number corresponding to this saturation of

ξ/λ_0 increase with N and with L_2/d. From Figs. 1. 4 (b) and (c), they are approximated for $L_2/d \geqq 70$ by

$$R_{ec}=1.9R_{ew}{}^{0.90}+2300, \quad (5\times10^4 \geqq R_{ew} \geqq 10^4) \tag{1.16}$$

which gives a fair agreement with the relationship between R_{ec} and R_{ew} obtained by Щукин[4].

1. 4. 2. Velocity Distributions

If the measured coefficient of hydraulic loss of long pipes, including rotating elements, ξ/λ_0, is plotted against the rotation rate, N, as shown in Fig. 1. 5 (b), the values of ξ/λ_0 are seen to be governed by a single parameter, N, when $L_2/d \geqq 100$. This can be explained by examining velocity profiles in the rotating pipe. Figure 1. 6 shows the velocity profiles in a rotating pipe of $120d$ downstream section, when $N=1.0$. At this section the influence of the pipe rotation on flow is considered to be saturated and all of the velocity profiles are similar.

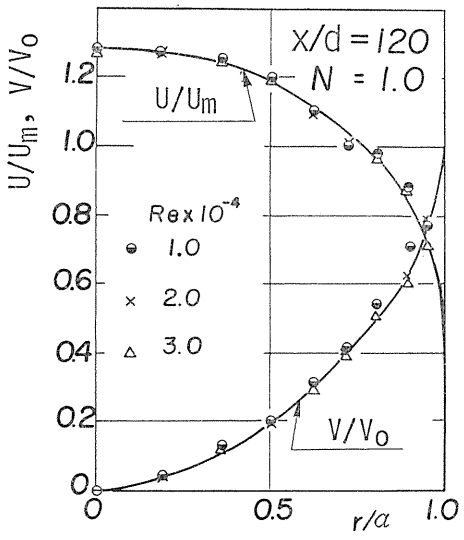

Fig. 1. 6 Similarity of velocity profiles at a constant value of N (N =1.0).

Velocity profiles change along the pipe. This is shown for various values of N by the data in Figs. 1.7 (a) and (b). Profiles measured at the section of x/d= 10 for $N=0$ are shown by broken lines. At $x/d=10$, the axial velocity profile remain flat and the flow in the greater part of the central zone is considered to be still in a turbulent state. As x/d increases, the axial velocity profiles deform gradually due to a stabilizing effect of the centrifugal force of the swirling flow.

Lavan and his co-workers[1] show theoretically that a reverse flow is to be expected near the wall at entry, for large N. In the present study, a tuft method did not show such a flow, within the range of $N \leqq 5$ and $R_e=10^5$.

At $100d$ or more downstream, the velocity profile becomes approximately independent of the axial distance from the inlet. For reference, the laminar velocity profile in a stationary pipe is shown by a chain line in Fig. 1.7 (b). To check the effect of the rotation rate, N was increased to 5. 8, 6. 8, and 8. 6 for $R_e=6.1\times$

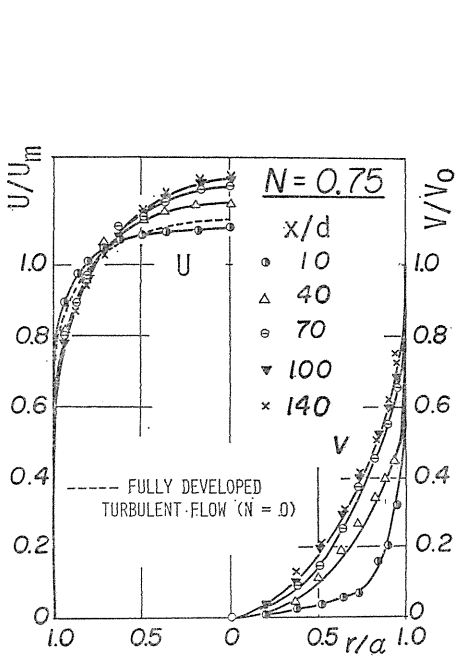

(a) $N=0.75$ and $R_e=2\times10^4$

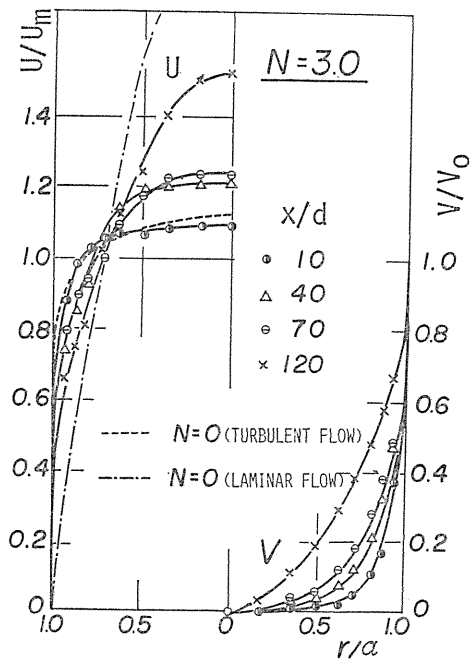

(b) $N=3.0$ and $R_e=2\times10^4$

Fig. 1. 7 Changes of velocity profiles along the pipe.

10^3, 5.1×10^3 and 4.6×10^3, respectively. The V profiles in these cases did not change appreciably from those shown in Fig. 1.7 (b) for $x/d=120$; they did not approach a forced-vortex type profile, even at the section far downstream of $x/d=120$. The U profiles remain approximately the same shape as in the laminar state, with the ratio of U_c to U_m at the pipe center equal to 1.72, 1.79, and 1.85 for $N=5.8$, 6.8, and 8.6, respectively[9].

1. 4. 3. Pressure Distributions

A dimensionless expression of pressure change within the rotating pipe can be given by

$$p=(P-P_0)/(\rho U_m^2/2) \qquad (1.17)$$

where P is a static pressure at any point in the section, and given by Eq. (1.12). Changes of pressure on the wall and at the center of the rotating pipe along the axis are shown in Fig. 1.8. Gradients of the pressure in a stationary pipe at the same Reynolds number are shown for turbulent and laminar conditions. Even with a low spin ratio of $N=0.25$, the pressure curves are seen to be affected considerably by the

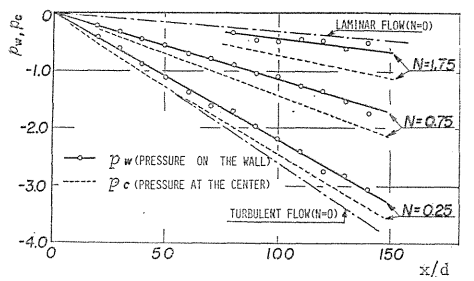

Fig. 1. 8 Changes of pressures on the wall and at the center of rotating pipe ($R_e=2\times10^4$).

rotation, and with increase of the rotation speed, the curve approaches asymptotically that of a laminar flow in a stationary pipe.

1. 4. 4. Shearing Stresses

From measured velocities and pressures, shearing stresses can be calculated by use of Eqs. (1.6) and (1.7). The results are shown in Figs. 1.9(a) and (b). The broken line in Fig. 1.9 (a) shows the values of τ_{rx} in the stationary state, the absolute value of which is slightly larger than in the rotating state.

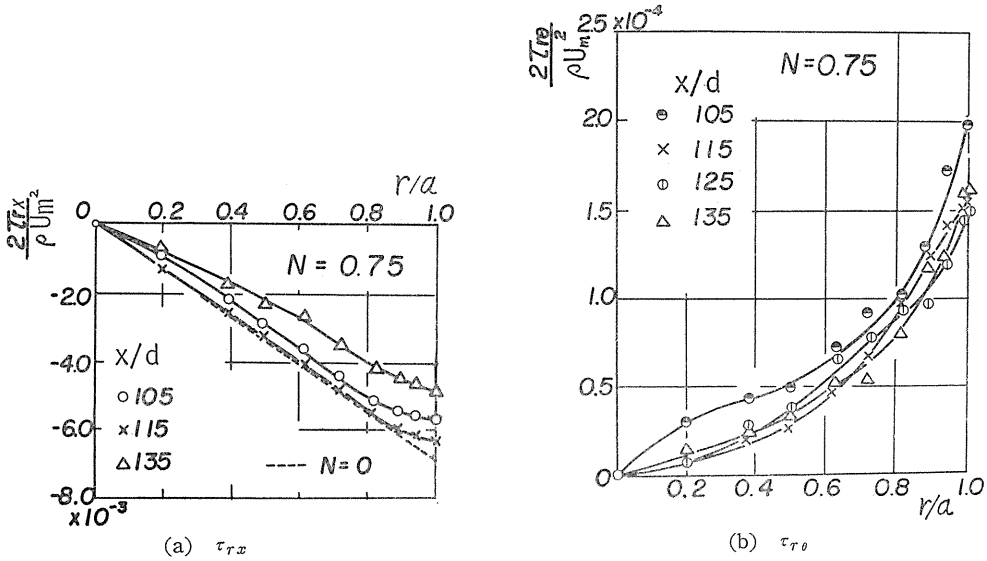

(a) τ_{rx} (b) $\tau_{r\theta}$

Fig. 1. 9 Distributions of shearing stresses (R_e=2×10⁴).

A dimensionless expression of the tangential component of the wall stress, $2(\tau_{r\theta})_0/(\rho U_m^2 N)$, for various values of R_e and R_{ew} is shown in a semilog scale in Fig. 1.10, showing that $2(\tau_{r\theta})_0/(\rho U_m^2 N)$ decays exponentially along the pipe axis. When N is small, the values are seen to be arranged well by a solid line, irrespective of the values of R_e and R_{ew}. This is to be expected from the fact that $2(\tau_{r\theta})_0/\rho U_m^2$ in Eq. (1.11) can be expressed by a product of N and the axial derivative of angular momentum flux in the rotating pipe. From the results in Fig. 1.10, $2(\tau_{r\theta})_0/(\rho U_m^2 N)$ can be approximated by, when $N \leqq 0.9$,

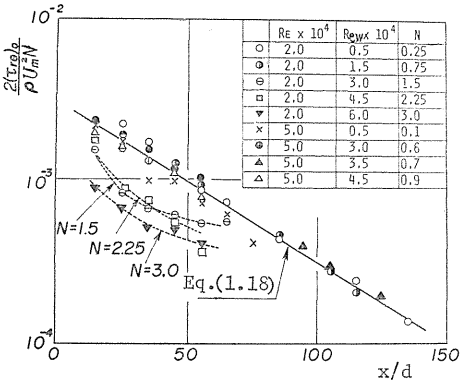

Fig. 1. 10 Changes of $2(\tau_{r\theta})_0/(\rho N U_m^2)$ along the pipe.

$$2(\tau_{r\theta})_0/(\rho U_m^2 N) = 0.00317 \exp[-0.023(x/d)] \qquad (1.18)$$

For $N>0.9$, an appreciable rate of suppression of turbulence will be expected in the inlet region of the rotating pipe and a larger reduction of $2(\tau_{r\theta})_0/(\rho U_m^2 N)$ will be observed.

1. 4. 5. Energy Fluxes in Rotating Pipe

Changes of E_t, E_k, and E_p along the pipe axis are calculated by Eqs. (1.3), (1.4), and (1.5) and the results are shown in Fig. 1.11. When N is increased, the rate of change in E_p is decreased, while that in E_k is increased. Thus, along the pipe axis the value of E_t is decreased for $N=0.25$ and 0.75 but is increased for $N=1.75$. This increase in E_t is due to the pipe rotation and it shows that the energy supplied by the pipe rotation is larger than that lost in the pipe. Most of the energies supplied in the rotating pipe is considered to be lost by wall friction in the downstream stationary pipe. Supply and consumption of energy will be performed by pipe wall through friction and both of them, having the opposite sign, may be considered to be roughly in the same magnitude, and the effect on the coefficient of hydraulic loss ξ is considered to be considerably small.

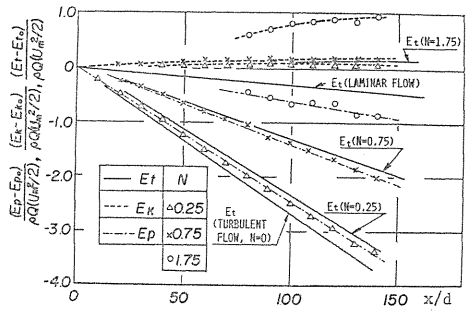

Fig. 11 Changes of E_p, E_k, and E_t along the pipe.

1. 5. Conclusions

Nonswirling turbulent flows were introduced to axially rotating pipes, and flow patterns and resistance in the pipes were investigated experimentally in the ranges of flow Reynolds number $10^4 \leqq R_e \leqq 2.0\times10^5$ and rotational Reynolds number $0 \leqq R_{ew} \leqq 6.5\times10^4$.

The results are summarized as follows:

(1) A swirling flow component given by the rotating pipe wall decreases the hydraulic loss undergone in the rotating pipes. The reduction in the hydraulic loss is a function of a parameter, $N=R_{ew}/R_e$, and the rotating pipe length. When the pipe length is larger than $100d$, the ratio of loss coefficient ξ/λ_0 is governed by a single parameter N. In this case ξ/λ_0 decreases as N increases from 0.35 to 1.2, and beyond this range the suppression of the turbulence is saturated and ξ/λ_0 remains substantially unaltered.

(2) Velocity profiles are governed by a parameter N and an axial distance from the rotating pipe inlet. With a constant value of N, the axial velocity distribution approaches the laminar flow profile in the downstream region, but the ultimate flow profile depends on the degree of turbulence suppression. Even when the spin ratio N was increased to 8.6, the measured velocity profiles exhibited neither a wholly laminar profile in the axial component nor a perfectly forced-vortex profile in the circumferential component.

2. Calculation of the Flow in Fully Developed Region

2. 1. Introduction

When a flow enters an axially rotating pipe, a swirling component of velocity is given to the flow by the moving wall and it causes large changes both in the time-mean velocity profiles and the turbulent structure of the flow, resulting in a change in the flow resistance.

The effects of the pipe rotation on the hydraulic loss have been investigated experimentally by many researchers[2), 3), 4)]. The present authors[10)] also measured the time-mean velocity components and hydraulic losses in axially rotating pipes when a fully developed turbulent flow was introduced into the pipe. The pipe rotation was found to suppress the turbulence in the flow, and also to reduce the hydraulic loss. The axial velocity in this case approaches a laminar flow type (parabolic) with an increase in the rotational speed of the pipe. The suppression of the turbulence due to the pipe rotation was also investigated in the boundary layer flow inside the rotating pipes when an undeveloped flow with a rectangular axial velocity distribution was introduced into them[11)].

Yamada and Imao[12)] measured the velocity profiles and hydraulic loss in a saturated downstream region of a rotating pipe when a fully turbulent flow was introduced into the pipe, and found the same kind of flow change as in the authors' study. When the inlet flow is laminar, however, the pipe rotation gives the opposite effects: the hydraulic loss is increased and the axial velocity profile tends to be a turbulent flow type.

The changes of the flow patterns in a rotating system in case of the turbulent flow entrance were calculated by Koosinlin, et al.[13)] using a modified mixing length theory, Aguilar and Pierce[14)] using an eddy viscosity model, and Launder, et al.[15)] using a two-equation model of turbulence. These calculations are those for the boundary layer flow developing not inside a rotating cylinder but outside a rotating body.

This chapter gives the results of calculations of velocity distribution and hydraulic loss in an axially rotating pipe in a region far downstream from its inlet section, where the effects of the rotation on the flow are supposed to be saturated. The calculation was performed, for the turbulent inlet condition, by use of a relationship between the mixing length and the Richardson number proposed by Bradshaw[16)], and the results were confirmed by experiments. For a laminar flow entrance, the calculation was reasonably modified and gave satisfactory results

2. 2. Theory

2. 2. 1. Governing equations of motion

When a flow from a stationary pipe is introduced into an axially rotating pipe, a saturated state of flow can be attained in the sections far downstream from the pipe inlet and in those sections the time-mean velocity profile remains unchanged toward downstream.

Using a cylindrical coordinate system as illustrated in Fig. 2. 1, the equations of motiom in the pipe can be written as follows:

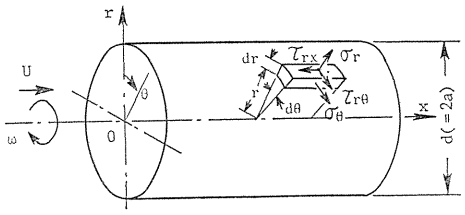

Fig. 2. 1 Cylindrical coordinate

$$-\frac{\partial P}{\partial x}=\frac{1}{r}\frac{\partial(r\tau_{rx})}{\partial r} \tag{2.1}$$

$$\frac{1}{r^2}\frac{\partial(r^2\tau_{r\theta})}{\partial r}=0 \tag{2.2}$$

$$-\frac{\rho V^2}{r}=\frac{1}{r}\frac{\partial(r\delta_r)}{\partial r}-\frac{\delta_\theta}{r} \tag{2.3}$$

where

$$\tau_{rx}=-\mu\partial U/\partial r-\rho\overline{uw} \tag{2.4}$$

$$\tau_{r\theta}=-\mu r\partial(V/r)/\partial r-\rho\overline{vw} \tag{2.5}$$

$$\delta_r=-P-2\mu\partial W/\partial r-\rho\overline{w}^2 \tag{2.6}$$

$$\delta_\theta=-P-\rho\overline{v}^2 \tag{2.7}$$

In the above equations (U, V, W) and (u, v, w) are the time-mean and turbulent components of velocities in x, θ, and r directions, respectively. Integration of Eq. (2.1) gives

$$\tau_{rx}=-(\partial P/\partial x)(r/2) \tag{2.8}$$

Introducing the friction coefficient of the pipe, λ, the pressure gradient along the pipe can be be expressed by the following equation,

$$-(\partial P/\partial x)=\rho\lambda U_m^2/4a \tag{2.9}$$

From Eqs. (2.8) and (2.9), $(\partial P/\partial x)$ can be eliminated and

$$\tau_{rx}/\rho=(\lambda/8)(r/a)U_m^2 \tag{2.10}$$

On the pipe wall $(\tau_{rx})_0$ becomes

$$(\tau_{rx})_0/\rho=(\lambda/8)U_m^2 \tag{2.11}$$

The equations (2.1) to (2.11) are also valid for a laminar state of flow, if the turbulent velocity components are made zero, namely $u=v=w=0$.

2. 2. 2. Mixing length model

(a) Turbulent flow entrance

Using Prandtl's mixing length theory, the axial shear stress τ_{rx} in Eq. (2. 10) can be represented as follows when the flow state is turbulent.

$$\tau_{rx}=-\mu\frac{\partial U}{\partial r}-\rho l^2\left[\left(\frac{\partial U}{\partial r}\right)^2+\left\{r\frac{\partial}{\partial r}\left(\frac{V}{r}\right)\right\}^2\right]^{1/2}\frac{\partial U}{\partial r} \tag{2.12}$$

where l is the mixing length. Substitution of Eq. (2. 10) into Eq. (2. 12) yields

$$l^2\left[\left(\frac{\partial U}{\partial r}\right)^2+\left\{r\frac{\partial}{\partial r}\left(\frac{V}{r}\right)\right\}^2\right]^{1/2}\frac{\partial U}{\partial r}=-\frac{\lambda}{8}U_m^2\frac{r}{a}-\nu\frac{\partial U}{\partial r} \tag{2.13}$$

For a fully developed turbulent pipe flow ($R_e\geqq 10^5$), the mixing length in a stationary pipe, l_0, has been expressed by the following equation.

$$\frac{l_0}{a}=\kappa\left\{0.35-0.2\left(\frac{r}{a}\right)^2-0.15\left(\frac{r}{a}\right)^4\right\} \tag{2.14}$$

where κ denotes the Kármán constant, and $\kappa=0.4$. If the flow Reynolds number is reduced under the limit, the value of the mixing length will deviate from that obtained by Eq. (2. 14), but the expression itself may be considered to be available even in a low Reynolds number range.

In a rotating system, the mixing length l may be changed by the effect of the centrifugal force. To express the degree of turbulence suppression due to the centrifugal force, the mixing length given by Eq. (2. 14) must be modified by using Bradshaw's formula as,

$$l/l_0=1-\beta R_i \tag{2.15}$$

where β is a constant, and R_i is the Richardson number defined by

$$R_i=\frac{2(V/r^2)\partial(rV)/\partial r}{(\partial U/\partial r)^2+\{r\partial(V/r)/\partial r\}^2} \tag{2.16}$$

In the above equations, both of R_i and mixing length are assumed to be functions of the axial and tangential components of velocities.

According to the experiments by the present authors[10] and also by Yamada and Imao[12], the profile of tangential velocity, V, in the rotating pipe does not exhibit an exact forced vortex type distribution even in the sufficiently downstream sections of $x/d\geqq 120$ if the inlet flow is turbulent. In this case a parabolic distribution as expressed by the following equation is available.

$$V/V_0=(r/a)^2 \tag{2.17}$$

To express the rotation rate of the pipe, a dimensionless value defined by the ratio of the peripheral speed of the pipe V_0 to the mean axial velocity of the flow U_m is introduced:

$$N=V_0/U_m \tag{2.18}$$

Substituting Eqs. (2. 17)and (2. 18) into Eq. (2. 16), the Richardson number can be

written as

$$R_i=\frac{6N^2(r/a)^2}{\{\partial(U/U_m)/\partial(r/a)\}^2+\{(r/a)N\}^2}$$

$$=\frac{6N^2r'^2}{\{\partial(U/U_m)/\partial r'\}^2+r'^2N^2} \tag{2.19}$$

where $r'=r/a$.

(*b*) *Laminar flow entrance*

Pedley[7] analyzed the stability of a laminar flow with a rigid rotation in a rotating pipe and showed that the pipe rotation had a destabilizing effect on the flow if the axial Reynolds number R_e was greater than 82.9. From the measured value of the hydraulic loss experienced in the rotating pipe, within the range of $R_e<2300$, it is ascertained that the flow changes gradually into a turbulent state as the rotational speed of the pipe is increased[12]. In order to express this destabilizing effect of the pipe rotation when a laminar flow is introduced, the second term on the right hand side of Eq. (2.12) must be retained. Then the mixing length l/l_0 is considered to be a function of the rotational Reynolds number R_{ew} and

$$l/l_0=f(R_{ew}) \tag{2.20}$$

In this case the distribution of the tangential component of velocity V can be assumed to be a forced-vortex type expressed as

$$V/V_0=r/a \tag{2.21}$$

2. 2. 3. Relations necessary for description of velocity distribution and friction coefficient

From Eq. (2.11) the friction velocity U_τ can be obtained as

$$U_\tau=\sqrt{(\tau_{rx})_0/\rho}=\sqrt{\lambda/8}\,U_m \tag{2.22}$$

With use of Eq. (2.22), Eq. (2.13) can be transformed into a dimensionless form as

$$\left(\frac{l}{a}\right)^2\sqrt{1+\left(\frac{Nr'U_m/U_\tau}{dU'/dr'}\right)^2}\left(\frac{dU'}{dr'}\right)^2-\frac{1}{R_{e\tau}}\left(\frac{dU'}{dr'}\right)-r'=0 \tag{2.23}$$

when the inlet flow is turbulent, and

$$\left(\frac{l}{a}\right)^2\left(\frac{dU'}{dr'}\right)^2-\frac{1}{R_{e\tau}}\left(\frac{dU'}{dr'}\right)-r'=0 \tag{2.24}$$

when the inlet flow is laminar. In the above equations, $\partial U'/\partial r'$ is replacad by dU'/dr' and $U'=U/U_\tau$, and $R_{e\tau}$ denotes a Reynolds number based on the friction velocity as

$$R_{e\tau}=U_\tau a/\nu \tag{2.25}$$

Noticing that both of Eqs. (2.23) and (2.24) are quadratic in terms of (dU'/dr') and that the coefficients of the term in the equations are given by Eqs. (2.14)～(2.16) for a turbulent flow entrance and by Eq. (2.20) for a laminar flow entrance, the gradient of the axial velocity (dU'/dr') can be determined at any radial position. With this value the velocity U' at any radial distance is given by

$$U'=\int_1^{r'}\left(\frac{dU'}{dr'}\right)dr'=\int_0^{z'}\frac{dU'}{dz'}dz' \tag{2.26}$$

where $z'=1-r'$. Integrating Eq. (2.26) across pipe section, a dimensionless value of the mean axial velocity, u_m, can be estimated by the following relation as

$$u_m=\frac{U_m}{U_\tau}=2\int_0^1 r'U'dr' \tag{2.27}$$

and the value of Reynolds number Re is given by

$$R_e\equiv U_m d/\nu=2R_{e\tau}u_m \tag{2.28}$$

Substituting Eq. (2.27) into Eq. (2.22), the friction coefficient, λ, is given by

$$\lambda=8/u_m^2 \tag{2.29}$$

2. 2. 4. Boundary conditions and methods of calculation

To compute the value of (dU'/dr') numerically from Eq. (2.23) or (2.24), the radius of pipe, a, is divided into one thousand equal parts. On the pipe wall $(r=a)$ the mixing length, l, becomes zero and dU'/dz' $(=-dU'/dr')$ becomes

$$dU'/dz'=(1-z')R_{e\tau} \tag{2.30}$$

This equation can be applied through the viscous sublayer adjacent to the pipe wall, and the dimensionless thickness of which is assumed to be the same as in the stationary pipe as

$$Z^+\equiv U_\tau z/\nu\leqq 11.6 \tag{2.31}$$

When a turbulent flow enters the rotating pipe, the value of β in Eq. (2.15) may be taken as 0.4 and 0.5, taking account of the experimental data described later. Much more different value of β has been found in the other studies: Koosinlin and his co-workers[13] found the result of $\beta=5$ for their study on the external flow around a rotating cylinder, and the present authors obtained the value of $\beta=2\sim3$ in the study on the boundary layer flow developing in a rotating pipe[17]. Compared with these data, the value of $\beta=0.4\sim0.5$, which is available in the present study, is much smaller.

In the case when a laminar flow is introduced into the rotating pipe, l/l_0 in Eq. (2.20) can be assumed to be given by the following equation.

$$l/l_0=0.012R_{ew}{}^{0.5} \tag{2.32}$$

In this case the flow in the region of $Z^+\leqq5.0$ is assumed to remain laminar due to the presence of a viscous sublayer near the pipe wall.

For the velocity profile and the friction coefficient of the pipe, λ, calculations can be made by using an assumed value of $R_{e\tau}$ corresponding to the given values of N, R_e and R_{ew}. Value of (dU'/dr') at any radial point can be obtained for this assumed value of $R_{e\tau}$, and with this value the axial Reynolds number can be calculated by use of Eqs. (2.27) and (2.28). The value of R_e calculated by this method may deviate from that of R_e given initially. If the differnce between these two values, namely ε, exceeds the value of $R_e/1000$, the above process of calculation is repeated with another corrected value of $R_{e\tau}$ until ε falls within the range $|\varepsilon| \leqq R_e/1000$.

2. 3. *Experimental apparatus*

In order to confirm the calculated results, experiments were carried out with hydraulically smooth pipes of two different diameters of $d=20.0$mm and 5.0mm. Figure 2.2 shows a schematic outline of the experimental apparatus. Water delivered from an overflow tank was led to a rectifying tank, upstream stationary pipe ($l_1=100d$), a rotating pipe and a downstream stationary pipe, successively. The rotating pipe was driven by a variable speed motor.

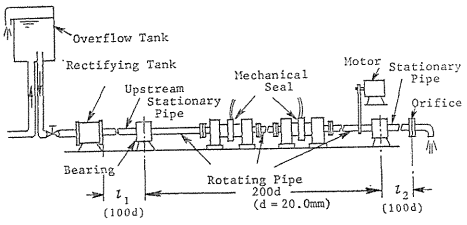

Fig. 2. 2 Schematic outline of experimental apparatus.

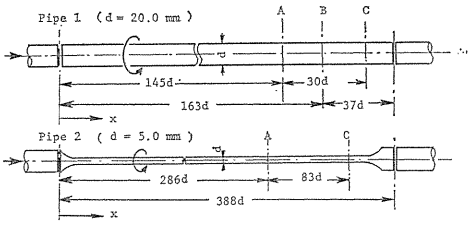

Fig. 2. 3 Detailed dimensions of rotating pipes and measuring sections.

Static pressure on the rotating pipe wall was introduced into a stationary system through the mechanical seals. Figure 2.3 shows the location of sections at which the hydraulic loss of the rotating pipes was measured. To exclude the effect of the inlet region on the pressure measurement, the pressure tappings were provided at the sections A ($x=145d$) and C ($x=175d$) on the pipe 1 ($d=20.0$mm), and A ($x=286d$) and C ($x=369d$) on the pipe 2 ($d=5.0$mm), respectively. With use of hydraulic loss of head, h_l, obtained from the static pressure difference between the two sections on each pipe, the friction coefficient, λ, can be evaluated by

$$\lambda = h_l / \{(l_r/d)(U_m^2/2g)\} \tag{2.33}$$

Employing a larger diameter pipe of $d=20.0$mm, the time-mean velocity components at the section $x=163d$ were measured by a laser doppler velocimeter. The measuring section was replaced by a lucite tube through which the laser beams could pass, and maximum 50ppm of milk was added as a tracer.

The axial Reynolds number R_e and the rotational Reynolds number R_{ew} were changed over the ranges of $500 \leqq R_e \leqq 2\times10^4$ and $0 \leqq R_{ew} \leqq 3.5\times10^4$, respectively.

2. 4. Comparison between theory and experiments

2. 4. 1. Turbulent flow entrance

(a) Velocity distributions

The calculated mean velocity profiles for the axial component U and the tangential velocity component V assumed by Eq. (2.17) are shown for $R_e=10^4$, 2×10^4, and 5×10^4 in Figs. 2.4 (a), (b), and (c), respectively, in which the experimental results for the same Reynolds numbers are also plotted for comparison. In this

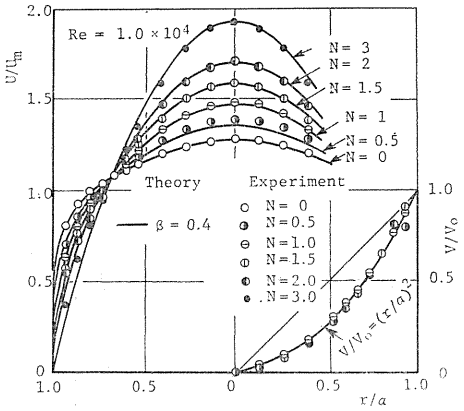

(a) $R_e=10^4$

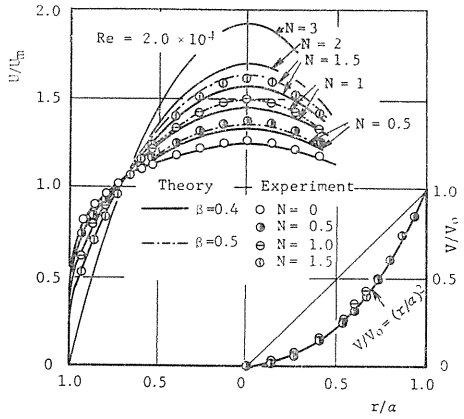

(b) $R_e=2\times10^4$

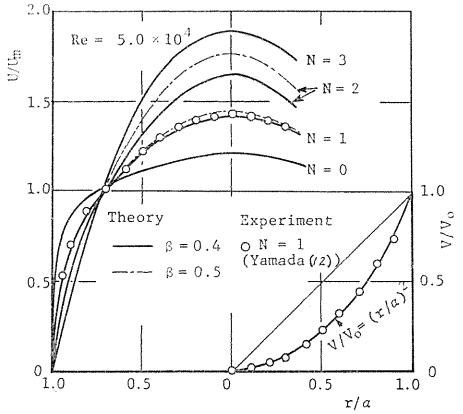

(c) $R_e=5\times10^4$

Fig. 2. 4 Velocity distributions for turbulent flow entrance.

calculation the mixing length, l, is determined from Eq. (2.15) with $\beta=0.4$. The results calculated with $\beta=0.5$ are also plotted in the same figures for reference. The thickness of the viscous sublayer in the calculations is taken to be $0\leqq Z^+\leqq 11.6$. When $R_e=10^4$ as indicated in Fig. 2.4 (a), the calculated profiles of the axial velocity are in close agreement with the experiments for all of the rotation rates within the range of $0\leqq N\leqq 3$. An examination of the velocity profiles U/U_m shows that they approach gradually a parabolic shape with an increase in N, and

correspondingly, the effect of turbulence suppression due to the pipe rotation becomes remarkable. When $R_e=2\times10^4$ (Fig. 2.4 (b)), the calculated velocity curves with $\beta=0.4$ (solid lines) have a little lower values than the measured curves in the central region of the pipe, and the difference increases by a slight amount as N is increased. The axial velocity profiles calculated with $\beta=0.5$ are also shown by the broken lines, the coincidence being better than the case with $\beta=0.4$. When $R_e=5\times10^4$ (Fig. 2.4 (c)), being a Reynolds number higher than the above, the calculated profiles with the values of $\beta=0.4$ and 0.5 agree fairly well with the experimental data obtained by Yamada et al., when $N=1.0$. The validity of the velocity profile assumption for the tangential component by Eq. (2.17) may be confirmed well in Figs. 2.4 (a), (b), and (c).

The dimensionless values of the maximum axial velocity, U_c/U_m, are plotted against N in Fig. 2.5. The values of U_c/U_m are seen to increase linearly with an increase in N within the range of $N>1$, and the agreement between the calculated and measured values is almost satisfactory ($\beta=0.4$). Though the calculated value of U_c/U_m decreases as R_e increases, the experimental data remain almost unchanged for different Reynolds numbers within the range $10^4\leqq R_e\leqq10^5$. When N exceeds about 3.5, the value of U_c/U_m may be taken to be constant i. e. 2, and the distribution of the axial velocities substantially displays a laminar flow pattern.

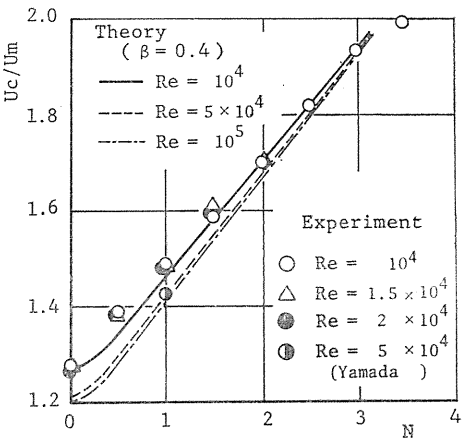

Fig. 2. 5 Relationship between U_c/U_m and N

(b) *Friction coefficients*

Figure 2.6 shows the relationship between the friction coefficient, λ, and the axial Reynolds number R_e. Solid and broken lines denote the calculated results for $\beta=0.4$ and 0.5, respectively. The value of λ calculated with $\beta=0.4$ exhibits a

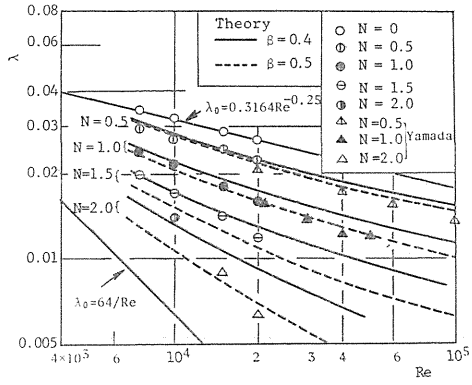

Fig. 2. 6 Friction coefficient of rotating pipe for turbulent flow entrance.

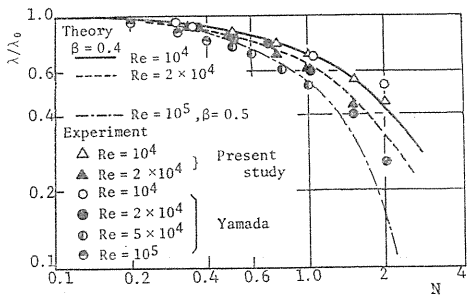

Fig. 2. 7 Relationship between λ/λ_0 and N.

little smaller value than with $\beta=0.5$. In this figure the measured values of λ are also plotted for various values of N. It may be found that the calculations of velocity profiles and friction coefficient yield fairly reasonable results, if a value of β in Eq. (2.15) is selected between 0.4 and 0.5.

The relationship between the friction coefficient λ and the rotation rate N is shown in Fig. 2.7, in which λ_0 is the friction coefficient of a stationary pipe. The values of λ/λ_0 decrease with an increase in N, and this tendency becomes remarkable for larger values of R_e. The data by the other researchers also show a satisfactory agreement with the calculated values in the present study.

(c) *Richardson number and mixing length*

The Richardson number R_i is evaluated from Eq. (2.19) when $R_e=10^4$, and its distributions across the pipe section are shown in Fig. 2.8. As the existence of the viscous sublayer near the pipe wall is assumed, the gradient of the axial velocity is given by the relationship $dU'/dr' = -R_{e\tau}r'$ and Richardson number R_i in this region remains constant and,

$$R_i=\frac{6N^2}{(2R_{e\tau}^2/R_e)^2+N^2}$$

On the other hand it tends to be zero at the pipe center. The value of R_i increases with an increase of N, and the curves of R_i are flattened over the greater part of the section.

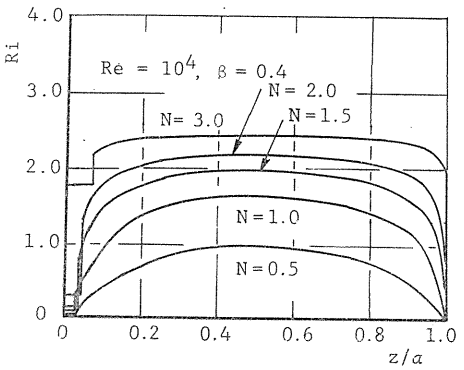

Fig. 2. 8 Distributions of Richardson numbers.

Figures 2.9 (a) and (b) show the distributions of l/a calculated by Eqs. (2.14) and (2.15) across the section. The values of l/a are taken to be zero in the

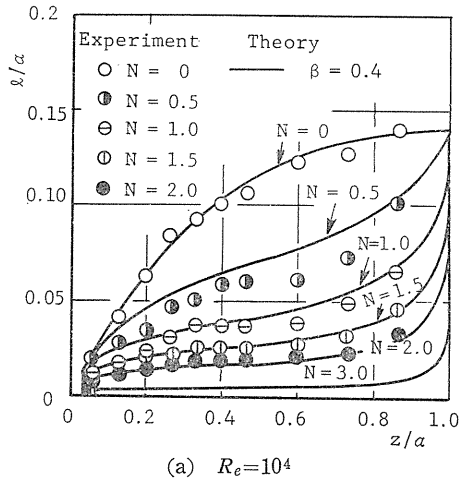

(a) $R_e=10^4$

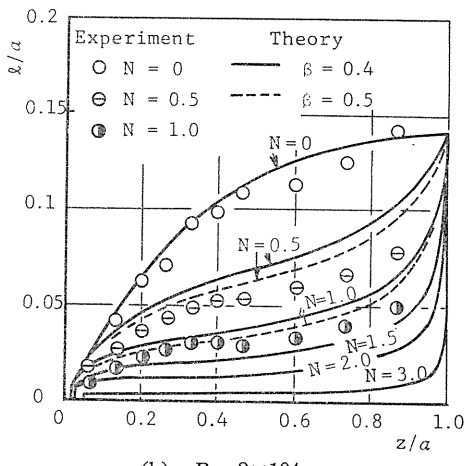

(b) $R_e=2\times10^4$

Fig. 2. 9 Distributions of l/a.

region $Z^+ \leqq 11.6$. The experimental values of l/a are those which are obtained from the relation of Eq. (2.13) using the measured values of the velocity gradient dU/dr and the friction coefficient λ. When $R_e=10^4$ (Fig. 2.9 (a)), the agreement between the calculated ($\beta=0.4$) and measured values is sufficient except for the case when $N=0.5$. The curves of l/a shift downward as N is increased, showing a greater suppression of turbulence for a larger value of N. A large reduction of l/a for $N=3$ corresponds to a flow relaminarization inside the rotating pipe and the value of U_c/U_m becomes approximately 1.9 as shown in Fig. 2.5. In Fig. 2.9 (b) the calculated results for $\beta=0.4$ and 0.5 are plotted when $R_e=2\times10^4$. The agreement with the experiments is better for $\beta=0.5$ than for $\beta=0.4$.

(d) Logarithmic velocity distribution

The wall law in the velocity distributions is checked in Fig. 2.10, where the calculated and experimental results for different R_e and N are plotted together. The agreement in the both data is fairly good except for the case of $N=1.0$. As is seen in this figure, the universality of the relationship between U/U_τ and Z^+ can be secured if N remains constant.

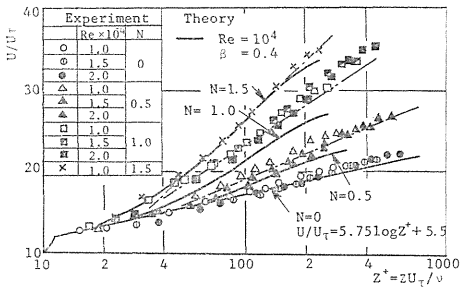

Fig. 2. 10 Logarithmic velocity distribution.

2. 4. 2. Laminar flow entrance

(a) Velocity distributions

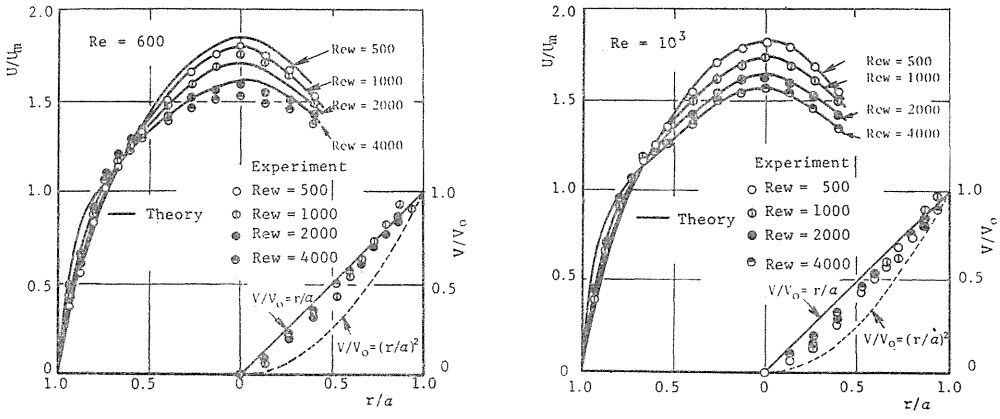

(a) $R_e=600$ (b) $R_e=10^3$

Fig. 2. 11 Velocity distributions for laminar flow entrance.

Figures 2. 11 (a) and (b) exhibit the effect of the pipe rotation on the velocity distributions when $R_e=600$ and 1000, respectively. When a laminar condition of flow is introduced into an axially rotating pipe, the flow will be disturbed by the rotating wall and become ultimately turbulent. Thus, with the use of a turbulent flow analogy, degree of the disturbance is assumed to be decided by a modified mixing length defined by Eq. (2. 32). The axial velocity profiles calculated by this method (when $R_e=10^3$) are compared with the experimental results in Fig. 2. 11 (b), showing a good coincidence. The coincidence, however, becomes a little poor in case of $R_e=600$, but their tendencies are quite similar. For more advanced calculations, another equation for the mixing length must be used instead of Eq. (2. 32).

Distribution of the tangential velocities in this flow shows a nearly forced vortex type profile ($V/V_0=r/a$) as is seen in Figs. 2. 11 (a) and (b), where a parabolic profile valid for the turbulent flow entrance is also plotted for comparison.

(*b*) *Friction coefficients*

Figure 2. 12 shows the relationship between the friction coeffficient λ and the rotational Reynolds number R_{ew} when a laminar flow is introduced. The value of λ is shown dimensionlessly by use of $\lambda_0=64/R_e$ available for a stationary pipe. The value of λ/λ_0 increases with R_{ew}, which corresponds to the change in the axial velocity profile. The calculated curve for $R_e=1000$ agrees well with the experimental results and with a fine solid curve by Yamada's empirical equation.

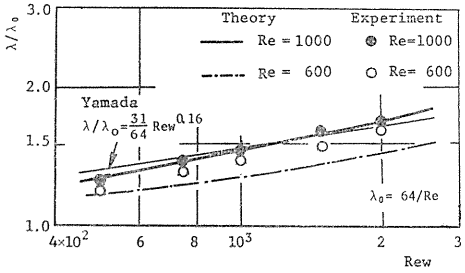

Fig. 2. 12 Relationship between λ/λ_0 and R_{ew} for laminar flow entrance.

2. 5. *Conclusions*

Calculations were made for a flow in the saturated region in an axially rotating pipe by using a modified mixing length theory and the results are compared with experiment. The following are the essentials:

(1) When a turbulent flow is introduced into a rotating pipe, changes in the velocity distribution and friction coefficient due to the tangential velocity given by the rotating wall can be accurately calculated with the value of $\beta=0.4\sim0.5$ in (2. 15). With an increase in N, the mixing length is decreased and becomes substantially zero when N exceeds 3. 5, at which the axial velocity profile changes into a laminar flow type.

(2) Destabilizing effect appears on a flow in a rotating pipe when a laminar flow is introduced into the pipe. Changes in velocity distribution and friction coefficient by this effect can be calculated by use of a modified mixing length, Eq. (2. 32).

3. Flow in Developing Region of Boundary Layer (Experiment and calculation)

3. 1. Introduction

When a flow enters an axially rotating pipe, a tangential velocity component is given to the flow by the moving wall and a three-dimensional boundary layer is formed in the rotating pipe. The development of the boundary layer along the pipe is affected by the rotating motion of the pipe. The effect of the pipe rotation on the flow has been studied by several investigators including the present authors[2, 5, 12, 18].

The present authors measured the time-mean velocity components and hydraulic losses of the pipe in the case where a fully developed flow was introduced into an axially rotating pipe in a turbulent flow state[18]. Pipe rotation was found to cause a drop in the hydraulic loss in the rotating pipe and to deform the axial velocity profile into a shape similar to that observed in a laminar flow. These changes are due to the stabilizing effect caused by the centrifugal force of the tangential flow component. According to the authors' study[19], when an undeveloped flow is introduced into the rotating pipe, the pipe rotation incurs two counter effects on the developing boundary layer flow: one is a destabilizing effect due to an increase of the relative velocity of the fluid at the surface of the rotating pipe, and the other is a stabilizing effect due to the turbulence suppression caused by the centrifugal force of the swirling flow component. The governing factors for the flow are the axial and tangential Reynolds numbers, and different combinations of two Reynolds numbers bring about different states of stability. But the detailed natures of the boundary layer, especially those of the turbulent intensity and the Reynolds shear stresses, have been left uninvestigated.

This chapter describes the experimental results on the time-mean volocities and Reynolds stress components inside the turbulent boundary layer in an axially rotating pipe when an undeveloped flow is introduced into it. Using the experimental results, the relationship between the mixing length and Richardson number proposed by Bradshaw[16] was also examined.

3. 2. Apparatus and method of experiment

A schematic outline of the experimental apparatus is shown in Fig. 3. 1 (a). Air discharged from a centrifugal blower was introduced into the rectifying tank. After the turbulence was made homogeneous over the inlet section of the rotating pipe by a honeycomb (20mm square and 100mm long) and six screens (mesh size: 1.0~2.62mm, screen wire dia. : 0.26~0.56mm), the air stream was throttled by the nozzle in the ratio of 12.3 : 1, which made the velocity profile at the inlet section of the rotating pipe almost uniform and the intensity of the turbulence was decreased less than 0.3 percent except for the small region near the pipe wall ($z/a \leqq 0.06$ for $R_e = 6 \times 10^4$).

In order to ensure that the flow state inside the boundary layer be turbulent just downstream of the inlet section, a step-ring of 1.0mm height was installed at the exit section of the nozzle as shown in Fig. 3. 1 (a). The turbulent state was ascertained by a hot-wire probe in the experimental range of the Reynolds number, $R_e = (6 \sim 9) \times 10^4$.

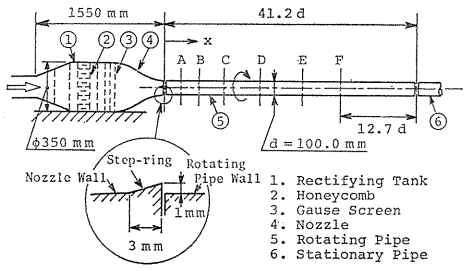

Fig. 3. 1 (a) Schematic outline of experimental apparatus.

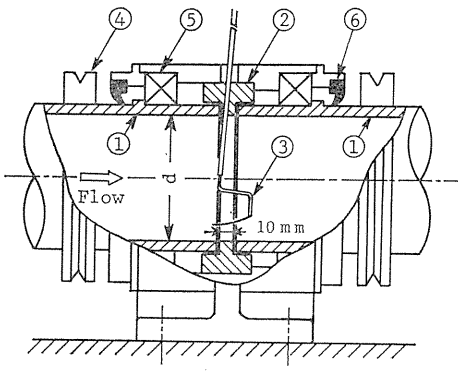

1. Rotating Pipes 2. Stationary Ring
3. Hot-wire Probe 4. Pulley
5. Bearing 6. Oil-seal

Fig. 3. 1 (b) Details in measuring section.

Measurements of the time-mean velocity components and the Reynolds stresses were made using the method of a rotated hot-wire[20,21]. Two types of hot-wire probes were employed; one was a straight hot-wire type (the wire element was set normal to the stem axis) and the other was a slanted hot-wire type (the wire element was mounted at an angle of about 45 degrees to the axis). The active length of the wires (5-micron tungsten) and the distance between the two prongs were 1 mm and 3 mm, respectively. These probes were inserted through a small hole drilled in a narrow stationary ring 10mm in length placed between two rotating sections. To avoid the effect of this stationary ring on the velocity profile in the boundary layer, the probes were inserted at an angle of 4 degrees from the perpendicular, as shown in Fig. 3. 1 (b).

Measurements were made at the sections of $x/d=2.7$, 5.7, 9.7, 15.5, 22.5, and 28.5, respectively, for the axial Reynolds number $R_e=6\times10^4$ and for the range of rotation rate $0\leqq N\leqq0.83$.

3. 3. Equations

3. 3. 1. Momentum and energy equations

Using the boundary-layer approximation, the equations of mean motion can be written in cylindrical coordinates for the case of an axisymmetric flow as follows:

$$U\frac{\partial U}{\partial x}+W\frac{\partial U}{\partial z}=-\frac{1}{\rho}\frac{\partial P}{\partial x}+\frac{1}{\rho r}\frac{\partial}{\partial z}(r\tau_{rx}) \tag{3.1}$$

$$U\frac{\partial V}{\partial x}+\frac{W}{r}\frac{\partial}{\partial z}(rV)=\frac{1}{\rho r^2}\frac{\partial}{\partial z}(r^2\tau_{r\theta}) \tag{3.2}$$

$$\frac{V^2}{r}=\frac{1}{\rho}\frac{\partial P}{\partial r}+\frac{1}{r}\frac{\partial}{\partial r}(r\overline{w^2})-\frac{\overline{v^2}}{r} \tag{3.3}$$

$$\frac{\partial}{\partial x}(rU)+\frac{\partial}{\partial z}(rW)=0 \tag{3.4}$$

where (U, V, W) and (u, v, w) are the time-mean and turbulent velocity components, respectively, in Fig. 3. 2. The shear stress components in both the axial and tangential directions, τ_{rx} and $\tau_{r\theta}$, are given by the following equations.

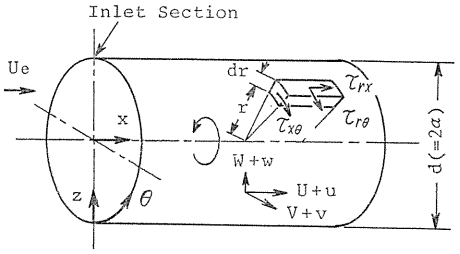

Fig. 3. 2 Cylindrical coordinate system.

$$\tau_{rx}=-\rho\overline{uw}+\mu\frac{\partial U}{\partial z},\quad \tau_{r\theta}=-\rho\overline{vw}+\mu r\frac{\partial}{\partial z}(V/r) \tag{3.5}$$

From Eqs. (3.1) and (3.2), the energy equations of the time-mean velocities can be obtained as:

$$U\frac{\partial}{\partial x}(U^2/2)+W\frac{\partial}{\partial z}(U^2/2)=-\frac{U}{\rho}\frac{\partial P}{\partial x}+\overline{uw}\frac{\partial U}{\partial z}-\frac{1}{r}\frac{\partial}{\partial z}(\overline{uwr}U)$$
$$-\nu\left(\frac{\partial U}{\partial z}\right)^2+\frac{\nu}{2r}\frac{\partial}{\partial z}\left(r\frac{\partial U^2}{\partial z}\right) \tag{3.6}$$

$$U\frac{\partial}{\partial x}(V^2/2)+W\frac{\partial}{\partial z}(V^2/2)=\frac{V^2W}{r}+\overline{vw}r\frac{\partial}{\partial z}(V/r)-\frac{1}{r}\frac{\partial}{\partial z}(\overline{vwr}V)$$
$$-\nu\left\{r\frac{\partial}{\partial z}(V/r)\right\}^2+\frac{\nu}{2r}\frac{\partial}{\partial z}\left\{r^3\frac{\partial}{\partial z}(V/r)^2\right\} \tag{3.7}$$

In the right-hand sides of Eqs. (3.6) and (3.7), the terms including the kinematic viscosity are negligibly small compared with the other terms except for the region of the viscous sublayler. Using the boundary-layer approximation, the turbulent energy equation can be expressed as:

$$U\frac{\partial}{\partial x}(q^2/2)+W\frac{\partial}{\partial z}(q^2/2)=-\overline{uw}\frac{\partial U}{\partial z}-\overline{vw}r\frac{\partial}{\partial z}(V/r)+D-\varepsilon \tag{3.8}$$

where D and ε denote the turbulent diffusion and the viscous dissipation of the energy, respectively. In the above equation the terms on the left-hand side correspond to the convection terms of the turbulent energy, and both the first and second terms on the right-hand side of the equation are the production terms. The second production term does not appear in the stationary state of the pipe.

3. 3. 2. Mixing length and Richardson number

Coefficients of the eddy viscosity both in the axial and tangential directions are defined by:

$$\nu_{tx}=-\overline{uw}\Big/\left(\frac{\partial U}{\partial z}\right),\qquad \nu_{t\theta}=-\overline{vw}\Big/\left\{r\frac{\partial}{\partial z}(V/r)\right\} \tag{3.9}$$

Using the values of the eddy viscosity, the mixing lengths in both directions can be expressed by the reference[13] as:

$$l_i^2=\nu_{ti}\Big/\left[\left(\frac{\partial U}{\partial z}\right)^2+\left\{r\frac{\partial}{\partial z}(V/r)\right\}^2\right]^{1/2},\quad i=x,\ \theta \tag{3.10}$$

From the analogy between the buoyancy and centrifugal force, Bradshaw[16] proposed the mixing length l as a function of the Richardson number in the field of a centrifugal force as follows:

$$l=l_0(1-\beta R_i) \tag{3.11}$$

where l_0 denotes the value of the mixing length in a flow with no swirl component, β is a constant, and R_i is the Richardson number defined by:

$$R_i=\frac{2V}{r^2}\frac{\partial}{\partial r}(rV)\Big/\left[\left(\frac{\partial U}{\partial z}\right)^2+\left\{r\frac{\partial}{\partial z}(V/r)\right\}^2\right] \tag{3.12}$$

The value of the angular momentum, rV, increases with the radial distance r in the rotating pipe, and hence $R_i\geqq 0$, which shows that the tangential velocity component has a stabilizing effect on the flow when there are no destabilizing effects from other sources.

3. 4. Experimental results and discussions

3. 4. 1. Time-mean velocity distributions

The time-mean velocity profiles at the section just downstream from the pipe inlet ($x/d=0.05$) under the stationary condition of the pipe are indicated in Fig. 3. 3, where the effect of the step-ring at the pipe inlet is also shown. The profiles both with and without the step-ring are almost uniform across the section, except for a narrow region near the pipe wall. The intensity of the turbulence in the uniform velocity zone was measured to be less than 0.3 percent.

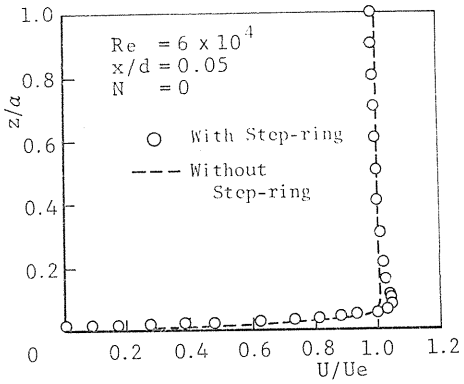

Fig. 3. 3 Velocity profile at the section just downstream from the pipe inlet ($x/d=0.05$) for $N=0$.

The similarity of the velocity profiles of the boundary layer in a stationary pipe when the step-ring is employed are shown in Fig. 3. 4 in which the velocity curve measured by Nikuradse in a fully developed turbulent pipe flow at $R_e=1.1\times10^5$ is also indicated.

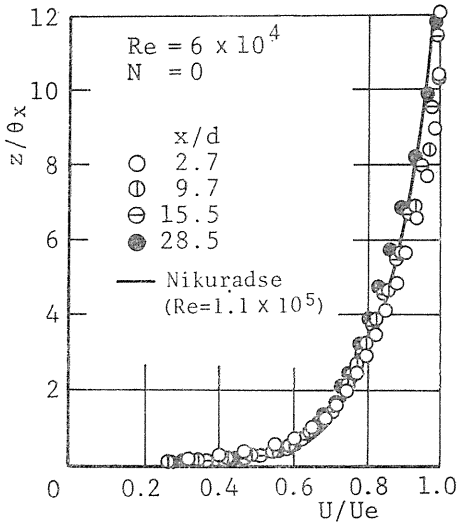

Fig. 3. 4 Velocity profiles for $N=0$.

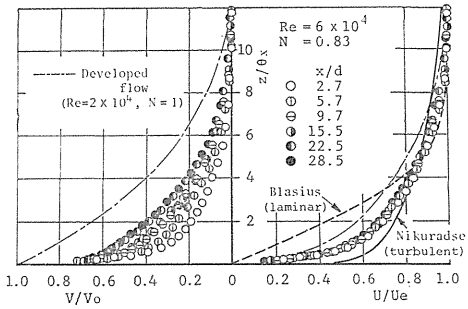

Fig. 3. 5 Changes in velocity profiles for $N=0.83$.

A fairly good coincidence in the velocity curves can be seen in the sections between $x/d=2.7$ and 28.5, and it may be considered that the flow in the boundary layer at the section of $x/d=2.7$ is already in a turbulent state when the step-ring is installed.

If the pipe is rotated, the velocity profiles are changed, an example of which is shown for $N=0.83$ in Fig. 3. 5, where the axial and tangential components of the velocities are plotted for different sections situated at $x/d=2.7\sim28.5$. In the same figure, the velocity profiles for a turbulent flow (Nikuradse) and a laminar flow (Blasius) in stationary ducts are also plotted for reference. The axial velocities at the different sections in the rotating pipe show a nearly similar profile, which lies between two reference velocity curves. As the section goes downstream, however, the tangential velocity curves are shifted upward in the inner region by the effect of the rotating wall. The effects of the rotation rate N on the velocity

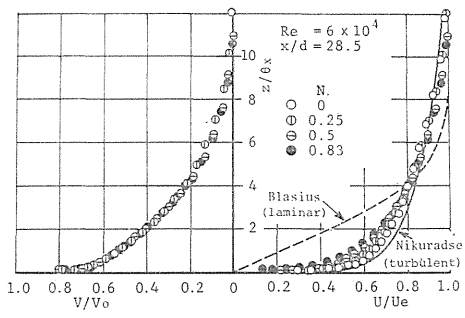

Fig. 3. 6 Changes in velocity profiles at the section $x/d=28.5$.

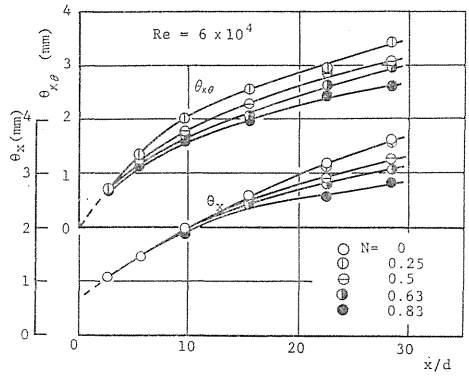

Fig. 3. 7 Development of momentum thickness along the pipe.

distributions at the section of $x/d=28.5$ are shown in Fig. 3.6. As the rotation rate increases, the axial velocity curves approach gradually to that in a laminar state as shown by a broken line. But, the tangential velocity profiles for each value of N remain almost unchanged. The tangential velocity curve can be approximated by the following equation:

$$1-V/V_0=\{(z/\theta_x)/10\}^{0.3}$$

The changes in the momentum thickness components along the pipe axis, θ_x and $\theta_{x\theta}$, are plotted in Fig. 3.7. As N increases, the curves of θ_x and $\theta_{x\theta}$ are flattened gradually, which displays the suppression of the boundary layer development due to the pipe rotation.

3. 4. 2. Turbulent fluctuations and Reynolds shear stresses

The distributions of the turbulent fluctuation velocities and Reynolds shear stresses in a section near the pipe inlet ($x/d=2.7$) are plotted in Figs. 3.8 (a) and (b), respectively. From Fig. 3.8 (a), it may be seen that the pipe rotation

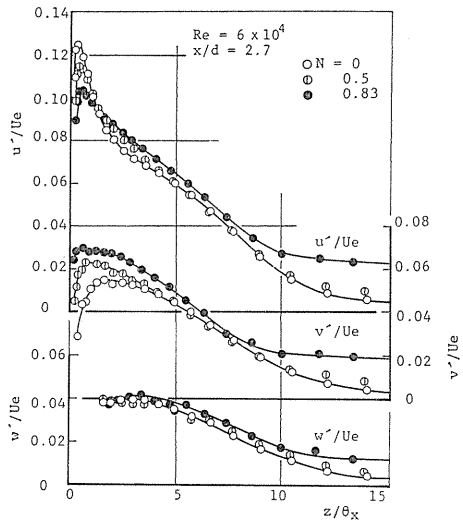

Fig. 3. 8 (a) Turbulent intensity components.

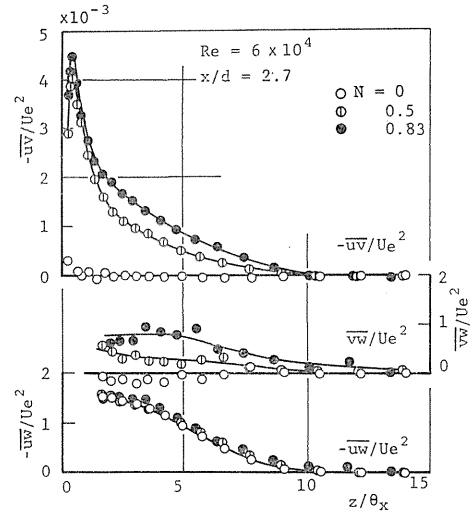

Fig. 3. 8 (b) Reynolds shear stresses.

gives a considerable change in the tangential component of the turbulent fluctuations but only a slight change in the axial and radial components. The Reynolds shear stress components $-\overline{uv}$ and $\overline{vw}$ in the stationary state of the pipe in Fig. 3.8 (b) are seen to be zero throughout the boundary layer as is expected from a statistical background. When the pipe is rotated, the stress components of $-\overline{uv}/U_e^2$ and $\overline{vw}/U_e^2$ increase with the increase of N, but the other component $-\overline{uw}/U_e^2$ remains almost unchanged. The increase in the Reynolds shear stress components is caused by an intense shear due to the rotational motion of the pipe wall, which prevails in the inlet region of the pipe.

Figures 3.9 (a) and (b) exhibit three components of the turbulent fluctuations

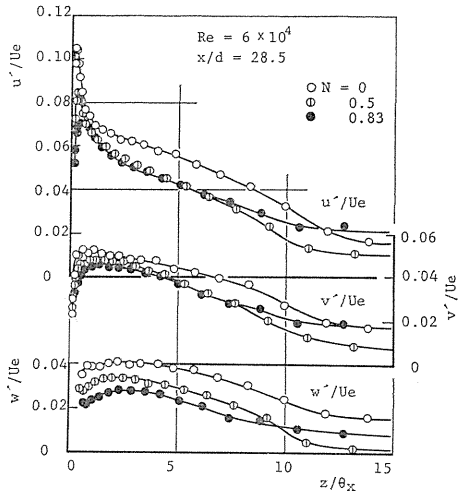

Fig. 3. 9 (a) Turbulent intensity components.

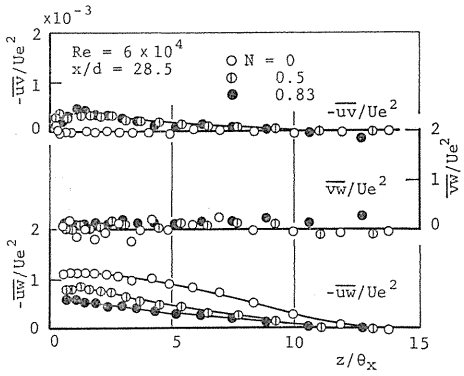

Fig. 3. 9 (b) Reynolds shear stresses.

and Reynolds shear stresses at the section of $x/d=28.5$, respectively. Unlike the results in the section of $x/d=2.7$, all of the fluctuation components in this section decrease with the increase in the rotation rate N. The drops in u'/U_e and v'/U_e are remarkable in the wall region $z/\theta_x \leqq 1$, but the decrease in w'/U_e is distributed uniformly across the boundary layer. Of the three Reynolds shear stresses, the effect of the pipe rotation on the stress $-\overline{uw}/U_e^2$ is evident, and it decreases with an increase in the rotation rate. The other stresses $-\overline{uv}/U_e^2$ and $\overline{vw}/U_e^2$, however, have only slight values in the rotational state as well as the stationary state.

Distributions of the kinetic energy of the turbulent fluctuation q^2/U_e^2 $(=(\overline{u}^2+\overline{v}^2+\overline{w}^2)/U_e^2)$ across the boundary layer are shown in Fig. 3.10. In the upstream section $x/d=2.7$, the turbulent energy is seen to increase with the rotational rate. This is due to an intense shear caused by the rotating wall. This destabilizing effect of the tangential shear, however, diminishes gradually as the section goes downstream, and the stabilizing effect due to the swirling flow becomes dominant. At the section $x/d=9.7$, all of energy curves fall nearly into a single curve because the stabilizing and destabilizing effects of the pipe rotation are well balanced. The drop in the turbulent energies in the downstream sections shows a dominant stabilizing effect caused by the centrifugal force of the swirling flow, and the turbulent energy in the rotating state becomes smaller than that in the stationary state. This fact corresponds well to the re-

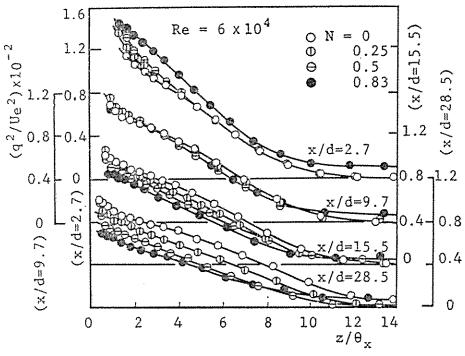

Fig. 3. 10 Distributions of turbulent energy.

sults in Fig. 3.7.

To estimate the contributions of each term in Eq. (3.8) to the entire turbulent energy, the values of each term for $x/d=2.7$ and 28.5 in $N=0.83$ are plotted in Figs. 3.11 (a) and (b), in which the first and second terms on the right-hand side of Eq. (3.8) are plotted in dimensionless forms as:

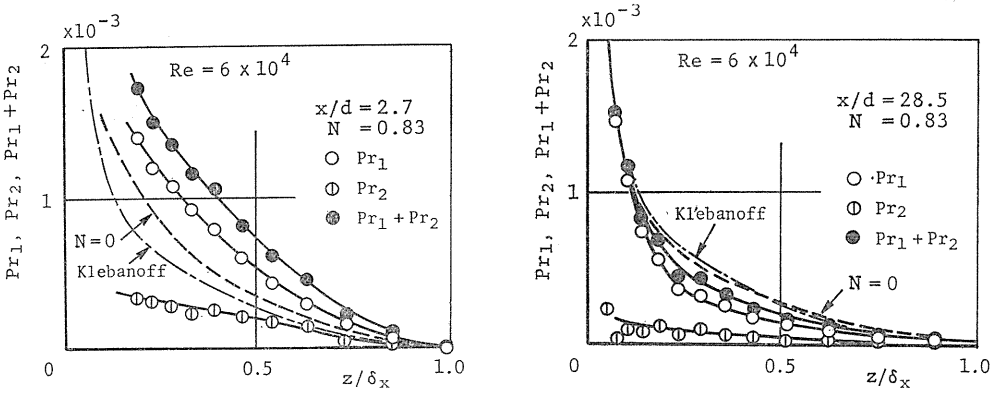

(a) At the section $x/d=2.7$ (b) At the section $x/d=28.5$

Fig. 3.11 Distributions of energy production terms ($N=0.83$).

$$P_{r1}=-\frac{\delta_x}{U_e^3}\overline{uw}\frac{\partial U}{\partial z},\quad P_{r2}=-\frac{\delta_x}{U_e^3}\overline{vwr}\frac{\partial}{\partial z}(V/r) \tag{3.13}$$

In these figures, the values of P_{r_1}, evaluated in this experiment at $N=0$, as well as those obtained by Klebanoff[22] in a turbulent boundary layer on a stationary flat-plate, are plotted for reference. At the section where $x/d=2.7$ (Fig. 3.11 (a)), the first production term P_{r_1} is greater than that observed for $N=0$, and the second production term P_{r_2}, which appears only in the rotating state, also has a small positive value. Consequently, the sum of the production terms, $P_{r_1}+P_{r_2}$, becomes much greater than the production term in the stationary pipe.

In the downstream section $x/d=28.5$ (Fig. 3.11 (b)), the production terms P_{r_1} and P_{r_2} have decreased greatly and their sum becomes smaller than the production term in the stationary state of the pipe. This decrease in the turbulent energy production in the rotating pipe corresponds well to the decrease in the turbulent fluctuation as shown in Figs. 3.9 (a) and (b).

Figure 3.12 shows the power spectra of the fluctuating velocity component in the mean flow direction. The data were measured at the point $z/\delta_x=0.2$ in the section $x/d=28.5$. The results in Fig. 3.12 are normalized as:

$$\int_0^\infty F(k)dk=1$$

where k is the wave number in the mean flow direction, i. e.

$$k=2\pi n/(U^2+V^2)^{1/2}$$

It is seen that the spectrum curves are flattened by an increase in the rotation

rate, hence the values of $F(k)$ increase in the range of higher wave number or smaller eddy range.

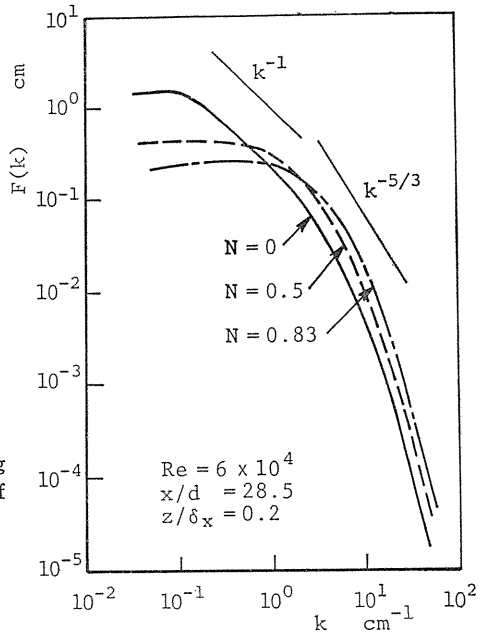

Fig. 3. 12 Power spectra of fluctuating velocity in the direction of mean flow.

3. 4. 4. Mixing length

Using the mixing length theory, the suppression of the turbulence due to pipe rotation can be equated with the decrease in the mixing length l_x. Figure 3.13 exhibits the distributions of l_x calculated by Eqs. (3.9) and (3.10) for various sections when $N=0$. Regardless of the axial distance, the mixing length can be expressed by the following relations:

$$l_x=0.4z, \quad \text{for } z/\delta_x<0.1$$

$$l_x=0.085\delta_x, \quad \text{for } z/\delta_x>0.35$$

The distributions of l_x at the sections $x/d=28.5$ and 15.5 in rotating states of the pipe are shown in Figs. 3.14 (a) and (b), respectively. In both sections, the mixing length decreases significantly with an increase in rotation rate, exhibiting the stabilizing effect due to pipe rotation. The gradient of the curves near the pipe wall decreases as N is increased. From an analogy of two forces, the buoyancy and the centrifugal force, Bradshaw[16] has expressed the mixing length in a rotating field as a function of the Richardson

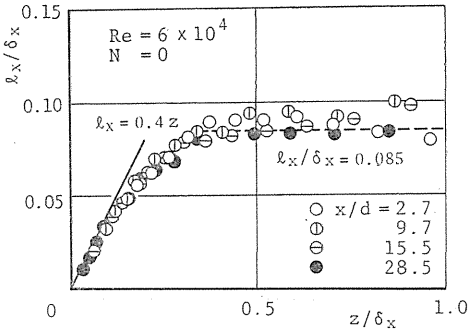

Fig. 3. 13 Distribution of mixing length for $N=0$.

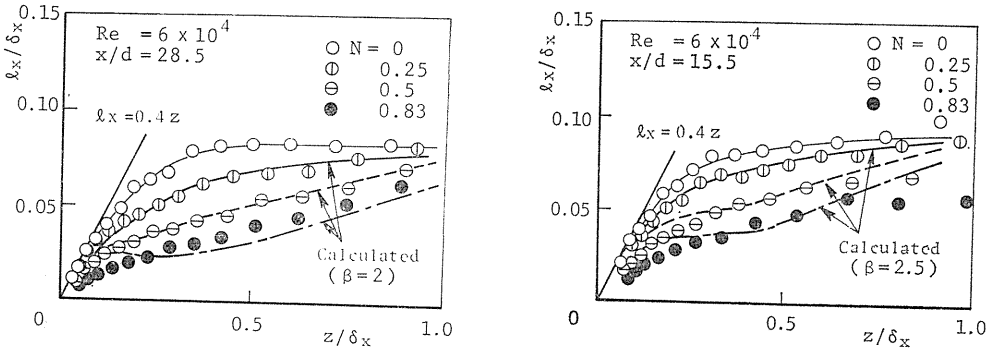

(a) At the section of $x/d=28.5$. (b) At the section of $x/d=15.5$.

Fig. 3. 14 Changes in mixing length due to rotation.

number R_i by Eq. (3.12). Using the values of R_i calculated by Eq. (3.12), the values of l_x in the sections of $x/d=28.5$ and 15.5 can be evaluated, and the results are compared with the experiments in Figs. 3.14 (a) and (b), where in the calculation β is taken as 2 and 2.5 for the two sections, respectively. It is seen that the calculated values agree well with the experiments.

For the discussion of the mixing length change in the curved or rotating flow, Bradshaw[16] has pointed out that the "flux" Richardson number, R_f, given by the following equation may be more appropriate than the "gradient" Richardson number, R_i, defined by Eq. (3.12).

$$R_f=2\overline{vw}(V/r)/\left\{-\overline{uw}\frac{\partial U}{\partial z}+\frac{\overline{vw}}{r}\frac{\partial}{\partial r}(rV)\right\} \tag{3.14}$$

The use of Eq. (3.14), however, is found not to be adequate in the present flow problem, because the tangential component of the Reynolds stresses, $\overline{vw}$, is much less than the axial component, $-\overline{uw}$, within the boundary layer at the section of $x/d=28.5$, as shown in Fig. 3.9 (b) and the value of R_f remains substantially zero for the rotation rate of $N=0\sim0.83$.

3. 5. Conclusions

(1) The rotation of a pipe generally suppresses development of the turbulent boundary layer in the pipe, and the time-mean axial velocity profile approaches the velocity curve of a laminar state with an increase in the rotational speed.

(2) In the sections immediately downstream from the pipe inlet ($x/d<10$), the Reynolds shear stress components $-\overline{uv}$ and $\overline{vw}$ are increased by an intensive shear due to the relative motion near the pipe wall.

(3) In the sections further downstream ($x/d\geqq10$), a stabilizing effect caused by the centrifugal force of the swirling flow develops in the rotating pipe, suppressing gradually the turbulence along the pipe. The turbulence intensity ultimately falls below that of the stationary state of the pipe.

(4) Changes in the mixing length due to the pipe rotation can be estimated by use of the Richardson number.

4. Nomenclature

a: pipe radius
d: pipe diameter
E_k: kinetic energy flux
E_p: pressure energy flux
E_t: useful energy flux
$F(k)$: normalized power spectrum in direction of mean flow
H: hydraulic loss between measuring sections located upstream and downstream of rotating pipe
h_l: hydraulic loss between two sections on rotating pipe
L_1: axial distance of upstream wall tap measured from the rotating pipe inlet
L_2: lengths of rotating pipe
L_3: axial distance of downstream wall tap measured from the rotating pipe exit
l: mixing length in rotating pipe
l_0: mixing length in stationary pipe
n: frequency
N: rotation rate $=V_0/U_m$, the reciprocal of Rossby number
P: time-mean static presure
P_0: staic pressure at the center of the inlet
p: dimensionless value of static pressure
R_e: axial Reynolds number $=U_m d/\nu$
R_{ec}: critical value of R_e
R_{ew}: rotational Reynolds number $=V_0 d/\nu$
$R_{e\tau}$: Reynolds number based on friction velocity $=U_\tau a/\nu$
R_i: Richardson number (Eq. 2.16)
U, V, W: time-mean velocity components in x, θ, and z direction
u, v, w: fluctuating velocity components in x, θ, and z direction
U_c: axial velocity at pipe center
U_e: free stream velocity
U_m: mean flow velocity
V_0: circumferential speed of rotating pipe
z: radial distance from pipe wall $=a-r$
δ_x: boundary layer thickness
θ_x: momentum thickness of boundary layer in x direction
$$=\int_0^{\delta_x}(U/U_e)(1-U/U_e)(r/a)\,dz$$
$\theta_{x\theta}$: momentum thickness of boundary layer in θ direction
$$=\int_0^{\delta_x}(U/U_e)(V/V_0)(r/a)^2\,dz$$
τ_{rx}, $\tau_{r\theta}$: shearing stress components in x and θ direction
$(\tau_{rx})_0$: values of τ_{rx} on the pipe wall
λ: coefficient of hydraulic friction of rotating pipe
λ_0: coefficient of hydraulic friction of stationary pipe
ξ: coefficient of hydraulic loss of rotating pipe
κ: Kármán constant

ν: kinematic viscosity
ρ: density

References

1) Lavan, Z., Nielssen, H., and Fejer, A. A., *"Separation and Flow Reversal in Swirling Flows in Circular Ducts,"* Physics of Fluids, Vol. 12, No. 9, 1969, pp. 1747-1757.
2) White, A., *"Flow of a Fluid in Axially Rotating Pipe,"* Journal of Mechanical Engineering Science, Vol. 6, No. 1, 1964, pp. 47-54.
3) Levy, F., *"Strömungserscheinungen in Rotierenden Rohren,"* Verein Deutscher Ingenieur Forschungsheft, No. 535, 1929, pp. 18-45.
4) Щукин, В. К., "Гидравлическое Сопротивление Вращающихся Труб," Инженерно-Физический Журнал, Vol. 12, No. 6, 1967, pp. 782-787.
5) Cannon, J. N., and Kays, W. M., *"Heat Transfer to a Fluid Flowing inside a Pipe Rotating about its Longitudinal Axis,"* Trans. ASME Journal of Heat Transfer, Vol. 91, No. 1, 1969, pp. 135-139.
6) Борисенко, А. И, Костиков, О. Н. и Чумаченко, В, И., "Экспериментальное Исследвание Турбулентых Характеристик Потока во Вращающемся Канале," Инженерно-Физический Журнал, Vol. 24, No. 6, 1973, pp. 1103-1108.
7) Pedley, T. J., *"On the Stability of Viscous Flow in a Rapidly Rotating Pipe,"* Journal of Fluid Mechanics, Vol. 35, No. 1, 1969, pp. 97-115.
8) Nagib, H. M., Wolf, L., Lavan, Z., and Fejer, A. A., *"On the Stability of the Flow in Rotating Pipes,"* Illinois Institute Technology Report, 1969.
9) Kikuyama, K., *"Experimental Investigation of Flow in Rotating Ducts,"* Doctoral Dissertation of Nagoya University, 1975 (in Japanese).
10) Murakami, M., et al. *"Flow of Fluid in a Pipe Rotating about its Longitudinal Axis,"* Trans. JSME, Vol. 42, No. 358, 1976, pp. 1784-1793 (in Japanese).
11) Murakami, M., Kikuyama, K. and Nishibori, K., *"Inlet Flow in a Rotating Pipe (1st Report, Development and Transition of Boundary Layer),"* Trans. JSME, Vol. 47, No. 424, B 1981, pp. 2274-2281 (in Japanese).
12) Yamada, Y. and Imao, S., *"Swirling Flow in an Axially Rotating Pipe,"* Trans. JSME, Vol. 46, No. 409, Ser. B, 1980, pp. 1662-1670 (in Japanese).
13) Koosinlin, M. L., Launder, B. E. and Sharma, B. I., *"Prediction of Momentum, Heat and Mass Transfer in Swirling, Turbulent Boundary Layers,"* Trans. ASME, Journal of Heat Transfer, Vol. 96, May, 1974, pp. 204-209.
14) Aguilar, F. and Pierce, F. J., *"Numerical Analysis of Turbulent Flow Along an Abruptly Rotated Cylinder,"* Trans. ASME, Journal of Fluids Engineering, Vol. 101, No. 2, 1979, pp. 251-258.
15) Launder, B. E., et al., *"The Calculation of Turbulent Boundary Layers on Spinning and Curved Surfaces"* Trans. ASME, ser. I, Vol. 99, No. 1, 1977, pp. 231-239.
16) Bradshaw, P., *"The Analogy between Streamline Curvature and Buoyancy in Turbulent Shear Flow,"* Journal of Fluid Mechanics, Vol. 36, No. 1, 1969, pp. 177-191.
17) Kikuyama, K., Murakami, M. and Nishibori, K., *"Development of Three-Dimensional Turbulent Boundary Layer in an Axially Rotating Pipe,"* Trans. ASME, Journal of Fluids Engineering, Vol. 105-2, 1983, pp. 154-160.
18) Murakami, M. and Kikuyama, K., *"Turbulent Flow in Axially Rotating Pipes,"* Trans. ASME Journal of Fluids Engineering, Vol. 102, No. 1, Mar. 1980, pp. 97-103.
19) Murakami, M., Kikuyama, K. and Nishibori, K., *"Three Dimensional Boundary Layer Development in an Axially Rotating Pipe,"* Proc. 3rd Symp. Turbulent Shear Flows, Calif. Univ. 1981, pp. 2.1-2.6.
20) Bissonnette, L. R. and Mellor, G. L., *"Experiments on the Behaviour of an Axisymmetric Turbulent Boundary Layer with a Sudden Circumferential Strain,"* Journal of

Fluid Mechanics, Vol. 63, 1974, pp. 369–413.
21) Nakamura, I., Yamashita, S. and Furuya, Y., *"Experiments on Turbulence Properties in the Thick Turbulent Boundary Layer on a Rotating Conical Body of Radius Decreasing Toward Downstream,"* Turbulent Shear Flows 2, ed. by J. S. Bradbury et al., Springer, 1980, pp. 99–115.
22) Klebanoff, P. S., *"Characteristics of Turbulence in a Boundary Layer with Zero Pressure Gradient,"* NACA Rpt. 1247, 1955.